

Nanostructured Biosensor for Measuring Neuropathy Target Esterase Activity

Neeraj Kohli,[†] Devesh Srivastava,[†] Jun Sun,[†] Rudy J. Richardson,[‡] Ilsoon Lee,^{*,†} and Robert M. Worden^{*,†}

Department of Chemical Engineering and Materials Science, Michigan State University, East Lansing, Michigan 48824, and Toxicology Program, Department of Environmental Health Sciences, School of Public Health, The University of Michigan, Ann Arbor, Michigan 48109-2029

Neuropathy target esterase (NTE) is a membrane protein found in human neurons and other cells, including lymphocytes. Binding of certain organophosphorus (OP) compounds to NTE is believed to cause OP-induced delayed neuropathy (OPIDN), a type of paralysis for which there is no effective treatment. Mutations in NTE have also been linked with serious neurological diseases, such as motor neuron disease. This paper describes development of the first nanostructured biosensor interface containing a catalytically active fragment of NTE known as NEST. The biosensor was fabricated using the layer-by-layer assembly approach, by immobilizing a layer of NEST on top of multilayers consisting of a polyelectrolyte (poly-L-lysine) and an enzyme (tyrosinase). The biosensor has a response time on the order of seconds and gives a concentration-dependent decrease in sensor output in response to a known NEST (and NTE) inhibitor. Potential applications of the biosensor include screening OP compounds for NTE inhibition and investigating the enzymology of wild-type and mutant forms of NTE. Although the development of a NEST biosensor was the primary purpose of this study, we found that the approach developed for NEST could also be extended to measure the activity of other esterases involved in neural processes, such as acetylcholinesterase (AChE) and butyrylcholinesterase (BChE). On the basis of measured sensitivities, phenyl valerate was the preferred substrate for NEST and BChE, whereas phenyl acetate was better for AChE.

Neuropathy target esterase (NTE), a membrane-bound serine esterase found in neurons of vertebrates,^{1–6} has been shown to

be necessary for embryonic development in mice and is believed to be involved in cell-signaling pathways and lipid trafficking.¹ The nucleophilic serine residue in NTE's active site attacks the carbonyl carbon atom of the substrate, forming a covalent acyl-enzyme intermediate, which is subsequently hydrolyzed. A consequence of this reaction mechanism is that the esterase activity of NTE is susceptible to covalent inhibition by organophosphorus (OP) esters, with which it forms an analogous phosphyl-enzyme intermediate. Irreversible binding of some OP compounds to the active serine site results in a debilitating neural disease known as OP-induced delayed neuropathy (OPIDN).¹ Symptoms of OPIDN include flaccid paralysis of the lower limbs, which becomes evident 2–3 weeks after exposure to neuropathic OP compounds. Recovery from this disease is usually poor, and there is no specific treatment. Because NTE is difficult to produce, research to study its esterase activity is typically done using a fragment of NTE that contains its esterase activity and can be more easily produced. One commonly used fragment, known as NEST, reacts with esters and inhibitors in a manner similar to NTE.^{3,4,7}

Widespread and long-term use of OP compounds in industry and agriculture has made these hazardous compounds a part of the environment, posing a health risk. In addition, neuropathic compounds could potentially be used as chemical weapons. Moreover, mutations in NTE have been linked to a complicated form of hereditary spastic paraplegia.⁸ Because of NTE's involvement in both chemically induced and spontaneously occurring neurological diseases, biosensors able to measure its esterase activity and inhibition by OP compounds would have important applications in medicine, toxicology, and homeland security.

Conventionally, the esterase activity of NTE (or NEST) is measured using a two-step process. First, the artificial substrate, phenyl valerate, is reacted with NEST or NTE to form phenol. Second, the concentration of phenol is determined either colorimetrically, in the presence of 4-amino antipyrine,⁹ or electrochemically, in the presence of tyrosinase.^{10,11} Tyrosinase converts phenol first to catechol and then to *o*-quinone, which can be measured

* Corresponding authors. E-mail: worden@egr.msu.edu (R.M.W.); leeil@egr.msu.edu (I.L.). Fax: (517) 432-1105.

[†] Department of Chemical Engineering and Materials Science, Michigan State University, East Lansing, MI 48824. Fax: (417) 432-1105

[‡] Toxicology Program, Department of Environmental Health Sciences, School of Public Health, The University of Michigan, Ann Arbor, MI 48109-2029.

(1) Glynn, P. *Biochem. J.* **1999**, *344*, 625–631.

(2) Li, Y.; Dinsdale, D.; Glynn, P. *J. Biol. Chem.* **2003**, *278*, 8820–8825.

(3) Atkins, J.; Glynn, P. *J. Biol. Chem.* **2000**, *275*, 24477–24483.

(4) Kropp, T. J.; Glynn, P.; Richardson, R. J. *Biochemistry* **2004**, *43*, 3716–3722.

(5) Makhaeva, G. F.; Sigolaeva, L. V.; Zhuravleva, L. V.; Eremenko, A. V.; Kurochkin, I. N.; Malygin, V. V.; Richardson, R. J. *J. Toxicol. Environ. Health, Part A* **2003**, *66*, 599–610.

(6) van Tienhoven, M.; Atkins, J.; Li, Y.; Glynn, P. *J. Biol. Chem.* **2002**, *277*, 20942–20948.

(7) Forshaw, P. J.; Atkins, J.; Ray, D. E.; Glynn, P. *J. Neurochem.* **2001**, *79*, 400–406.

(8) Rainier, S.; Bui, M.; Ming, L.; Plein, E.; Thomas, D.; Tokarz, D.; Delaney, C.; Albers, J. W.; Richardson, R. J.; Fink, J. K. Presented at the American Society of Human Genetics, Annual Meeting, Salt Lake City, UT, 2005.

(9) Kayyali, U. S.; Moore, T. B.; Randall, J. C.; Richardson, R. J. *J. Anal. Toxicol.* **1991**, *15*, 86–89.

(10) Sigolaeva, L. V.; Makower, A.; Eremenko, A. V.; Makhaeva, G. F.; Malygin, V. V.; Kurochkin, I. N.; Scheller, F. W. *Anal. Biochem.* **2001**, *290*, 1–9.

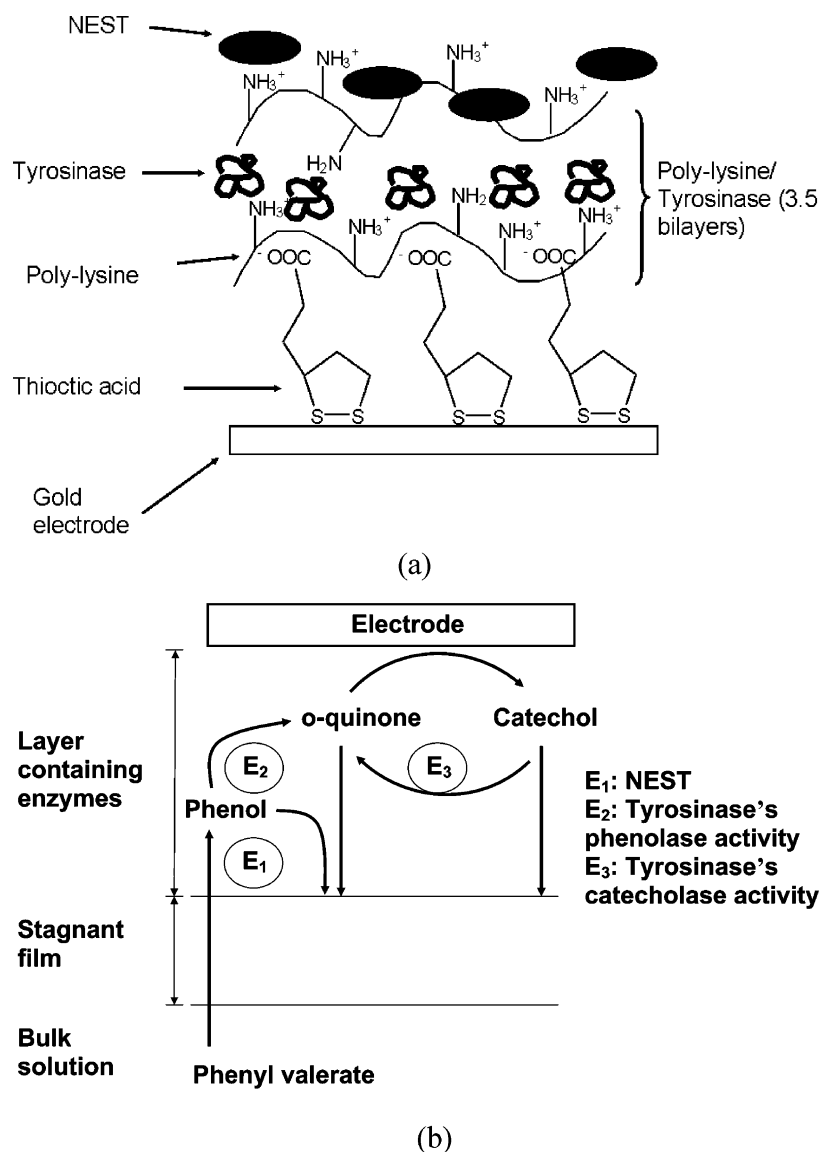


Figure 1. (a) Molecular architecture of the NEST biosensor. (b) Schematic representation of the pathway that leads to the generation of current in the NEST biosensor.

activity to be measured indirectly via measurement of *o*-quinone reduction at the electrode. The molecular architecture of the bienzyme sensor interface is shown schematically in Figure 1a. Gold electrodes cleaned in Piranha solution (seven parts by volume concentrated sulfuric acid and three parts by volume 30% hydrogen peroxide) were dipped in 5 mM solution of thioctic acid in ethanol for 30 min. The electrodes were washed with ethanol, dried under nitrogen, and dipped in PLL solution for 45 min. The PLL solution was prepared by adding 12 mg of PLL in 50 mL of 20 mM phosphate buffer (pH 8.5). The electrodes were then rinsed with water and dipped in an aqueous solution of Tyr (0.2 mg/mL) for 1 h. The last two steps were repeated 3.5 times to create 3.5 PLL–Tyr bilayers with PLL being the topmost layer. The electrodes were washed with water and dipped in a solution of NEST protein (0.1 mg/mL) in 100 mM phosphate buffer, pH (7.0) for 1 h. The electrodes were then washed with water, dried

under nitrogen, and dipped in phosphate buffer (0.1 M, pH 7.0) for testing. All the steps were done at room temperature.

Preparation of the Gold Electrode for Measuring the Activity of AChE and BChE. AChE and BChE were immobilized using the same procedure as for the NEST biosensor, except that the final dipping was done in a 0.1 mg/mL solution of AChE or BChE instead of NEST.

Electrochemical Impedance Spectroscopy. Electrochemical impedance spectroscopy (EIS) was performed using a CHI 660B electrochemical analyzer (CH instruments, Austin, TX). After deposition of each layer the gold working electrode was immersed in 10 mM [Fe(CN)₆]^{3-/4-} (1:1), in phosphate buffer, pH 7.0. The impedance spectra were obtained by sweeping an applied potential of 10 mV from 0.1 Hz to 10⁴ Hz, superimposed on a dc offset equivalent to an open-circuit potential. The impedance spectra were analyzed using Z-view software (version 2.1b, Scribner Associates, Southern Pines, NC).

Ellipsometry. Ellipsometric measurements were performed with a rotating analyzer ellipsometer (model M-44; J.A. Woollan

(19) Coche-Guerente, L.; Labbe, P.; Mengeaud, V. *Anal. Chem.* **2001**, *73*, 3206–3218.

(20) Forzani, E. S.; Solis, V. M.; Calvo, E. J. *Anal. Chem.* **2000**, *72*, 5300–5307.

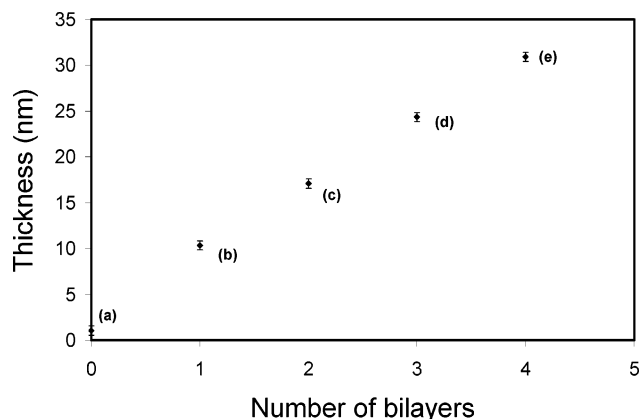


Figure 2. Ellipsometric thicknesses after the successive addition of the following layers: thioctic acid (point a), PLL–Tyr first bilayer (point b), PLL–Tyr second bilayer (point c), PLL–Tyr third bilayer (point d), and PLL–NEST final bilayer (point e).

Co. Inc., Lincoln, NE) running WVASE32 software. The thickness values for dried films were determined using 44 wavelengths between 414.0 and 736.1 nm. The angle of incidence was 75° for all experiments. Refractive indices of films containing PLL and proteins were assumed to be $n = 1.5$ and $k = 0$. These optical constants compare well with those determined in our lab for four bilayer films consisting of PLL and Tyr using ellipsometry.

Potential Step Voltammetry and Other Measurements.

The enzyme-modified electrodes were immersed in a stirred buffer solution and maintained at a potential of -100 mV (vs a Ag/AgCl reference electrode) using a BAS CV-50W electrochemical analyzer. The NEST esterase activity was measured indirectly via the electrode's output current for a variety of phenyl valerate concentrations. As shown in Figure 1b, the first step involves the diffusion of phenyl valerate through a stagnant film from bulk to the enzyme layer. The NEST enzyme then converts phenyl valerate to phenol, which is then oxidized to *o*-quinone by Tyr. Reduction of *o*-quinone at the electrode's surface generates a current and also regenerates catechol, which can then be reoxidized by Tyr. This internal recycling between catechol and *o*-quinone provides a mechanism for signal amplification and, hence, enhanced biosensor sensitivity.

To measure inhibition of NEST esterase activity, a known quantity of phenylmethylsulfonyl fluoride (PMSF) was added to the phosphate buffer (pH 7.0) under stirred conditions, and the resulting drop in current was measured. Unless otherwise stated, all the errors reported in this paper are the standard deviation (σ) values determined using 10 different electrodes.

RESULTS AND DISCUSSIONS

Ellipsometry and EIS. Ellipsometry and EIS were used to confirm deposition of the layers that make up the NEST biosensor. As shown in Figure 2, the thickness of the first PLL–Tyr bilayer was approximately 9.3 ± 0.4 nm, and that of the next two PLL–Tyr bilayers was approximately 7.2 ± 0.3 nm each. The thickness of the final PLL–NEST bilayer was approximately 6.6 ± 0.3 nm. The total thickness of the biosensor interface is about 30 nm.

EIS analysis was performed to provide further evidence of biosensor interface assembly and to study the electrical properties of the layers composing the interface. Figure 3i shows the Nyquist plots obtained on a bare gold electrode following the successive

addition of the following layers: thioctic acid (curve a), PLL–Tyr first bilayer (curve b), PLL–Tyr second bilayer (curve c), PLL–Tyr third bilayer (curve d), and PLL–NEST final bilayer (curve e).

All the Nyquist plots could be fit with the Randles equivalent circuit^{21,22} shown in Figure 3ii. This circuit produces a semicircle at higher frequencies that is related to the parallel double layer capacitance (C_{dl}) and charge-transfer resistance (R_{ct}). For this system, the R_{ct} value is approximately equal to the diameter of the semicircle. At lower frequencies, a straight line results that is related to the Warburg-diffusion impedance (Z_w). In other words, at high frequencies (short time scales), the impedance is controlled by electron-transfer kinetics, and at low frequencies (long time scales), the impedance is diffusion-controlled. The R_{ct} value is thought to be controlled by the thickness of the multilayered polymer assembly.^{21,22}

The Randles equivalent circuit model was fit to impedance plots to obtain R_{ct} , C_{dl} , Z_w , and solution resistance, R_s , values. The average best-fit values of R_{ct} are shown in Table 1. As expected, the R_{ct} increased upon the successive addition of layers, because each layer contributes additional resistance to electron transfer between the conductive support and the soluble redox probe.

Amperometric Response. Dependence of Biosensor Current on Working Potential and pH. The applied potential that optimized the biosensor's current was determined. Figure 4a shows the steady-state current in the presence and absence of phenyl valerate for applied potentials between 0.05 and -0.20 V. The highest signal-to-background ratio was obtained at -0.1 V. Therefore, a working potential of -0.1 V was used for further studies.

The effect of pH was also studied in the pH range of 5.5–8.0 in 0.1 M phosphate buffer at a working potential of -0.1 V. As shown in Figure 4b, the current was maximal at pH 7.0, so this pH value was used for subsequent studies.

Measurement of Esterase Activity using the NEST Biosensor.

Figure 5a shows a typical biosensor's response to successive addition of phenyl valerate aliquots, each sufficient to increase the concentration by $4 \mu\text{M}$. The well-defined step increases in current indicated a response time of less than 10 s. The biosensor's rapid response is due to the nanoscale thickness of the layers composing the interface. The current increased linearly with phenyl valerate concentration ($R^2 = 0.981$) in the range of 0.5– $12 \mu\text{M}$, and it reached saturation at about $30 \mu\text{M}$ (Figure 5b). The limit of detection was $0.5 \mu\text{M}$ at a signal-to-noise ratio of 3. The reproducibility of the sensor was investigated at a phenyl valerate concentration of $4 \mu\text{M}$; the mean current was approximately 348 nA cm^{-2} , with a standard deviation of approximately 10% ($n = 10$ electrodes). Figure 6 shows results of a control experiment done using an electrode containing the PLL and Tyr bilayers but no NEST. The response to $8 \mu\text{M}$ phenyl valerate was only about 2% of that obtained when the NEST layer was present. The small increase in signal may be due to trace amounts of phenol produced by autohydrolysis of phenyl valerate in solution.

This primary goal of this study was to develop a biosensor that could measure NEST activity and inhibition; three PLL–tyr layers and one NEST layer gave sufficient sensitivity to accomplish

(21) Pardo-Yissar, V.; Katz, E.; Lioubashevski, O.; Willner, I. *Langmuir* **2001**, *17*, 1110–1118.

(22) Harris, J. J.; Bruening, M. L. *Langmuir* **2000**, *16*, 2006–2013.

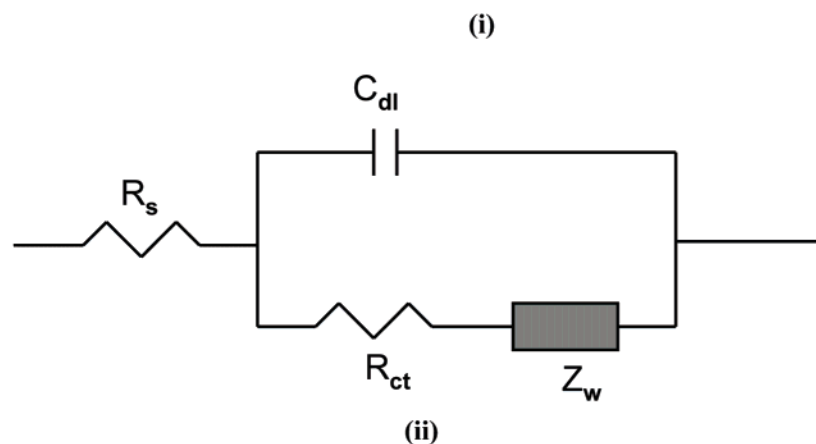
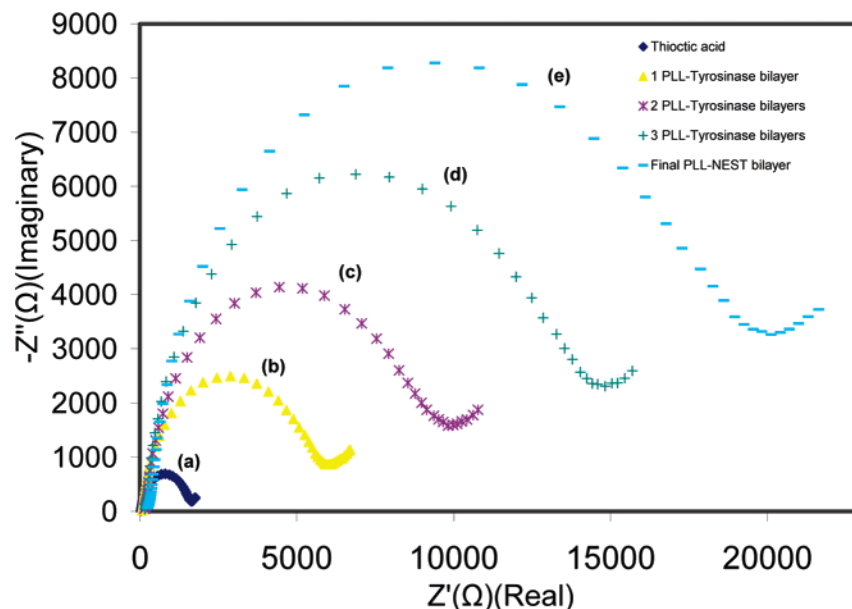


Figure 3. (i) Faradaic impedance spectra obtained on a bare gold electrode following the successive addition of following layers: thioctic acid (curve a), PLL-Tyr first bilayer (curve b), PLL-Tyr second bilayer (curve c), PLL-Tyr third bilayer (curve d), and PLL-NEST final bilayer (curve e). The impedance measurements were made in 0.1 M phosphate buffer, pH 7.0, in the presence of 1:1 10 mM $[\text{Fe}(\text{CN})_6]^{3-/4-}$. Geometric area of the electrode = 0.16 cm^2 . (ii) Randles equivalent circuit consisting of double layer capacitance (C_{dl}), charge-transfer resistance (R_{ct}), solution resistance (R_s), and Warburg impedance (Z_w).

Table 1. Average Best-Fit R_{ct} ($n = 10$ Electrodes) Values for Different Layers Present on the Gold Electrode^a

different layers	average R_{ct} ($\Omega \text{ cm}^2$)
thioctic acid	270 ± 60
thioctic acid-(PLL-Tyr) ₁	990 ± 150
thioctic acid-(PLL-Tyr) ₂	1570 ± 190
thioctic acid-(PLL-Tyr) ₃	2334 ± 220
thioctic acid-(PLL-Tyr) ₃ (PLL-NEST) ₁	3150 ± 300

^a The values were obtained by fitting the experimental data (Figure 3) to the equivalent circuit shown in Figure 3b using Z-view.

this goal. However, preliminary results (data not shown) indicate that the biosensor's sensitivity can be increased by increasing the number of NEST and Tyr layers, thus providing a means to optimize the biosensor's response characteristics for particular applications.

Amperometric Response to Catechol and Phenol. Because Tyr can convert both catechol and phenol to quinone, the response of the NEST biosensor to these compounds was also studied. Figures 7a and 8a show the current-time response curves after the successive addition of aliquots of phenol and catechol, respectively. Figures 7b and 8b show the corresponding phenol and catechol calibration curves. The response to phenol was linear ($R^2 = 0.980$) in the range of 1–25 μM , with an average sensitivity ($n = 10$ electrodes) of approximately $0.41 \pm 0.03 \mu\text{A } \mu\text{M}^{-1} \text{ cm}^{-2}$, and the current reached saturation at approximately 70 μM . The response to catechol was linear ($R^2 = 0.982$) in the range of 1–40 μM , with an average sensitivity ($n = 10$ electrodes) of $2.5 \pm 0.1 \mu\text{A } \mu\text{M}^{-1} \text{ cm}^{-2}$, and the current reached saturation at approximately 80 μM .

Inhibition of Esterase Activity. The biosensor's response to PMSF, a non-neuropathic compound previously shown to inhibit NEST (or NTE) esterase activity, was measured. The sensor was immersed in stirred phosphate buffer, and an aliquot of phenyl

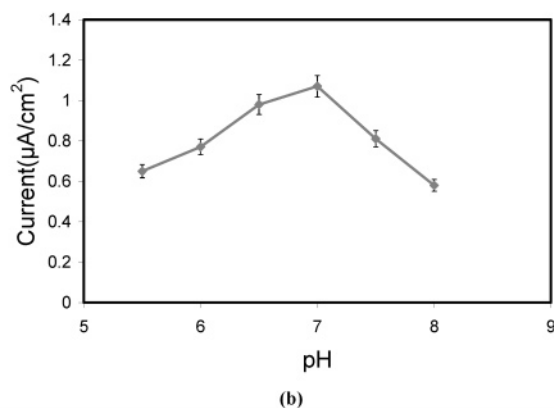
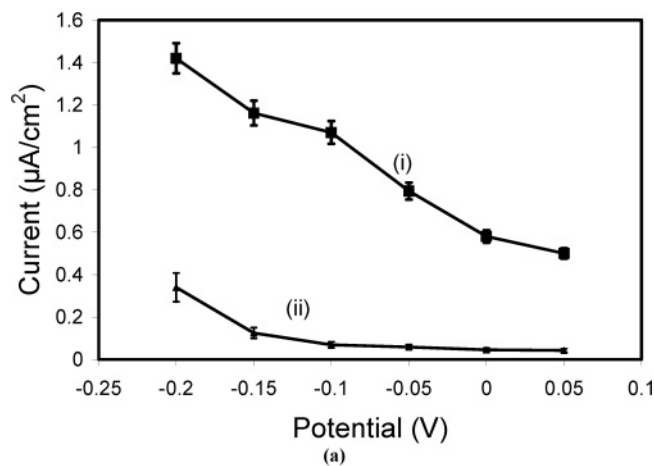


Figure 4. (a) Effect of working potential on the response current of the enzyme electrode in 0.1 M phosphate buffer (pH 7.0) with (i) and without (ii) 12 μM phenyl valerate solution, in 0.1 M phosphate buffer, at an applied potential of -0.1 V (vs Ag/AgCl). All the errors are standard deviations of five experiments. (b) Effect of pH on the response current of the bienzyme electrode in 0.1 M phosphate buffer containing 12 μM phenyl valerate solution at an applied potential of -0.1 V (vs Ag/AgCl). All the errors are standard deviations of five experiments.

valerate was added. After a steady biosensor signal was obtained, a known quantity of PMSF was added to the buffer. As shown in Figure 9, there was no decrease in current following addition of 10 μM PMSF, a $20\% \pm 3\%$ decrease following addition of 100 μM PMSF, and a $70\% \pm 4\%$ decrease on the addition of 1000 μM PMSF. PMSF inhibition of NEST esterase activity decreases the rate of phenol production and, consequently, the rate of *o*-quinone production. Therefore, less *o*-quinone is reduced at the electrode surface, leading to a drop in current. These results suggest that the NEST biosensor can be used for concentration-dependent detection of NEST (or NTE) inhibitors.

Control experiments to study the effect of PMSF addition on the response of the NEST biosensor to phenol and catechol were also performed. As expected, addition of PMSF had a negligible effect on the detection of phenol or catechol (data not shown), indicating that PMSF does not inhibit Tyr or poison the gold electrode in the concentration range studied.

Storage Stability. The biosensor's storage stability was tested by storing it at 4°C in phosphate buffer, pH 7.0, and measuring its response to a phenyl valerate standard solution daily. The activity remained stable for a week and then declined gradually, with a half-life of 15 days.

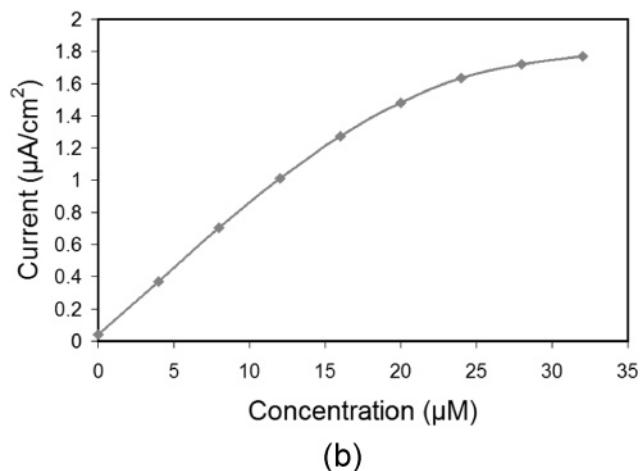
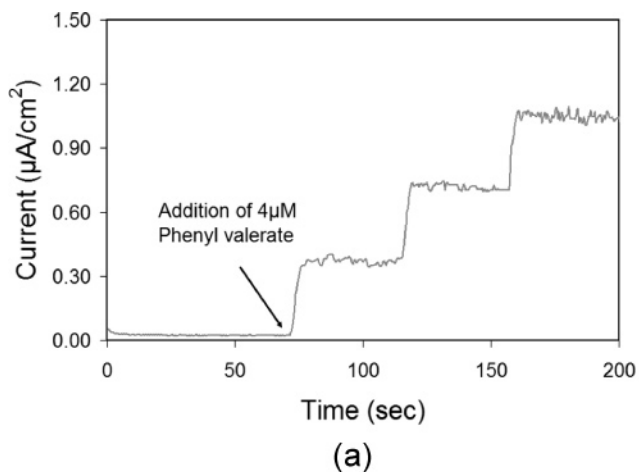


Figure 5. (a) Current vs time response of the NEST biosensor to the addition of aliquots of phenyl valerate to obtain final phenyl valerate concentrations as increments of 4 μM , in 0.1 M phosphate buffer, pH 7.0, at an applied potential of -0.1 V (vs Ag/AgCl). (b) Representative example of a calibration plot.

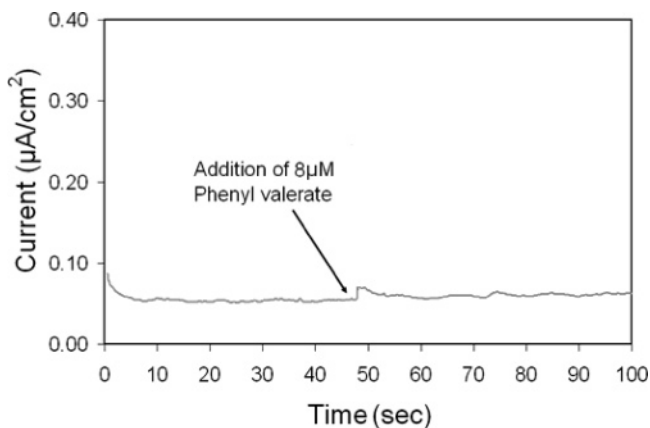
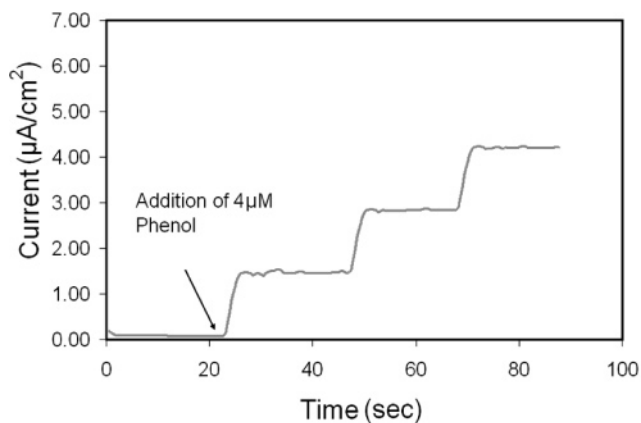
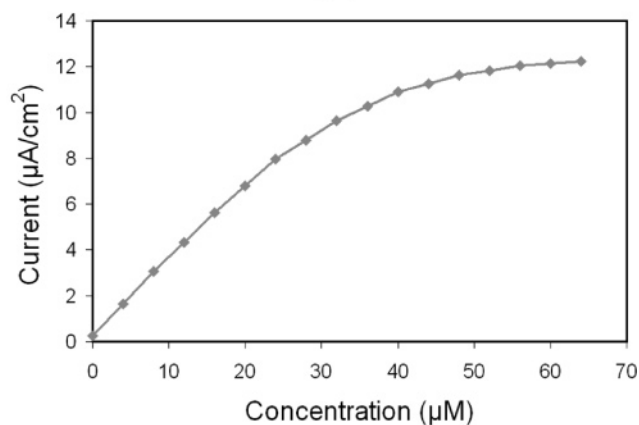


Figure 6. Control experiment: Current vs time response on an electrode containing only Tyr. The electrode was assembled in exactly the same way as the NEST biosensor, except that the final NEST layer was not deposited.

Immobilization of AChE and BChE. Although development of the NEST biosensor was the primary purpose of this study, we found that the same PLL-Tyr multilayer interface could also be used to immobilize and measure the activity of other esterases, such as AChE and BChE. Figure 10 displays a typical current–



(a)

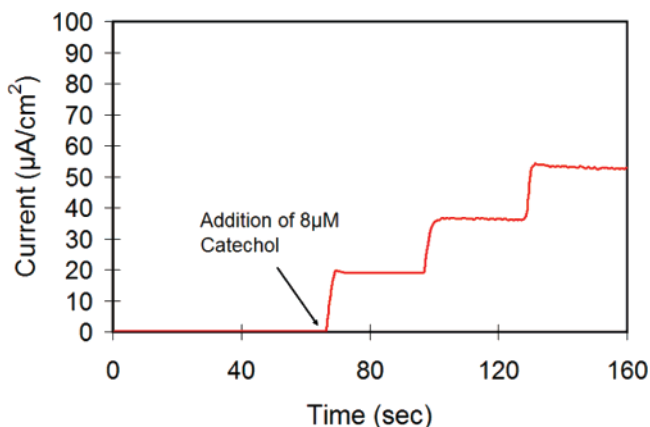


(b)

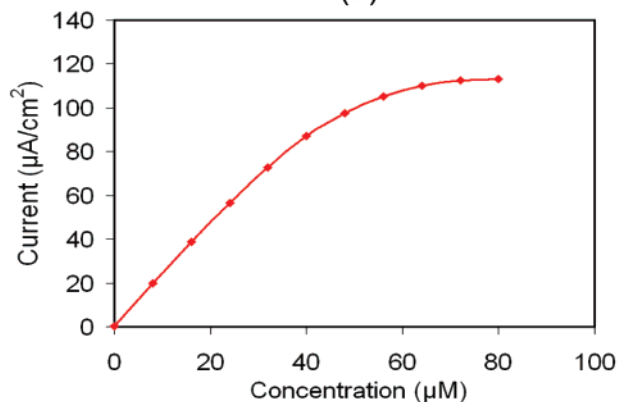
Figure 7. (a) Current vs time response of the NEST biosensor to the addition of aliquots of phenol to obtain final phenol concentrations as increments of $4 \mu\text{M}$, in 0.1 M phosphate buffer, pH 7.0, at an applied potential of -0.1 V (vs Ag/AgCl). (b) Representative example of a calibration plot.

time response curve for a bienzyme electrode containing Tyr and AChE after successive addition of aliquots of phenyl acetate to the phosphate buffer. The current increased linearly with the phenyl acetate concentration ($R^2 = 0.989$) in the range of $0.5\text{--}16 \mu\text{M}$ (data not shown), and it reached saturation at approximately $40 \mu\text{M}$. No significant rise in current was observed when phenyl valerate was used as a substrate, suggesting that phenyl acetate is a much better substrate for AChE than phenyl valerate. Current versus time response curves similar to those of Figures 5 and 10 were also obtained with bienzyme electrodes containing Tyr and BChE. However, for this interface, higher current sensitivity was obtained for phenyl valerate than for phenyl acetate. Table 2 summarizes the current sensitivities obtained with the three bienzyme interfaces. Control experiments were also done in which each of the substrates was delivered to a gold electrode containing only PLL-Tyr bilayers. The current sensitivities obtained in these control experiments were always less than $0.5 \text{ nA } \mu\text{M}^{-1} \text{ cm}^{-2}$.

Significance of the NEST Biosensor. This NEST-containing biosensor offers several advantages over the conventional, two-step method for measuring NEST (or NTE) activity. First, it requires only a single step—addition of the substrate phenyl valerate and/or an inhibitor—to measure the NEST activity. The



(a)



(b)

Figure 8. (a) Current vs time response of the NEST biosensor to the addition of aliquots of catechol to obtain final catechol concentrations as increments of $8 \mu\text{M}$, in 0.1 M phosphate buffer, pH 7.0, at an applied potential of -0.1 V (vs Ag/AgCl). (b) Representative example of a calibration plot.

biosensor's signal was shown to be proportional to the concentration NEST's rate-limiting substrate and inhibited by the known NEST inhibitor PMSF in a dose-dependent manner. Second, the nanometer-scale thickness of layers composing the interface provides a short diffusion path, yielding a rapid response time (less than 10 s). Third, the biosensor is suitable for continuous, real-time measurements of esterase activity, making it suitable for environmental monitoring applications. Fourth, the biosensor incorporates a signal amplification mechanism via recycling of o -quinone to catechol, which increases the biosensor's sensitivity. Fifth, the fabrication method, layer-by-layer self-assembly, is suitable for miniaturization and readily adaptable to microfluidic systems, enabling the production of high-density biosensor arrays for high-throughput applications.

The NEST-containing biosensor is well suited for several important applications, including studying the kinetic properties of NEST and other esterase enzymes involved in neurological processes. Example applications include detecting the presence of neuropathic agents that target NTE, screening OP compounds for inhibition of NTE, AChE, or BChE, and studying the kinetics of NTE's esterase activity. Moreover, the approach can in principle be extended to full length NTE, allowing the effects of mutations on NTE's enzymatic properties to be studied.

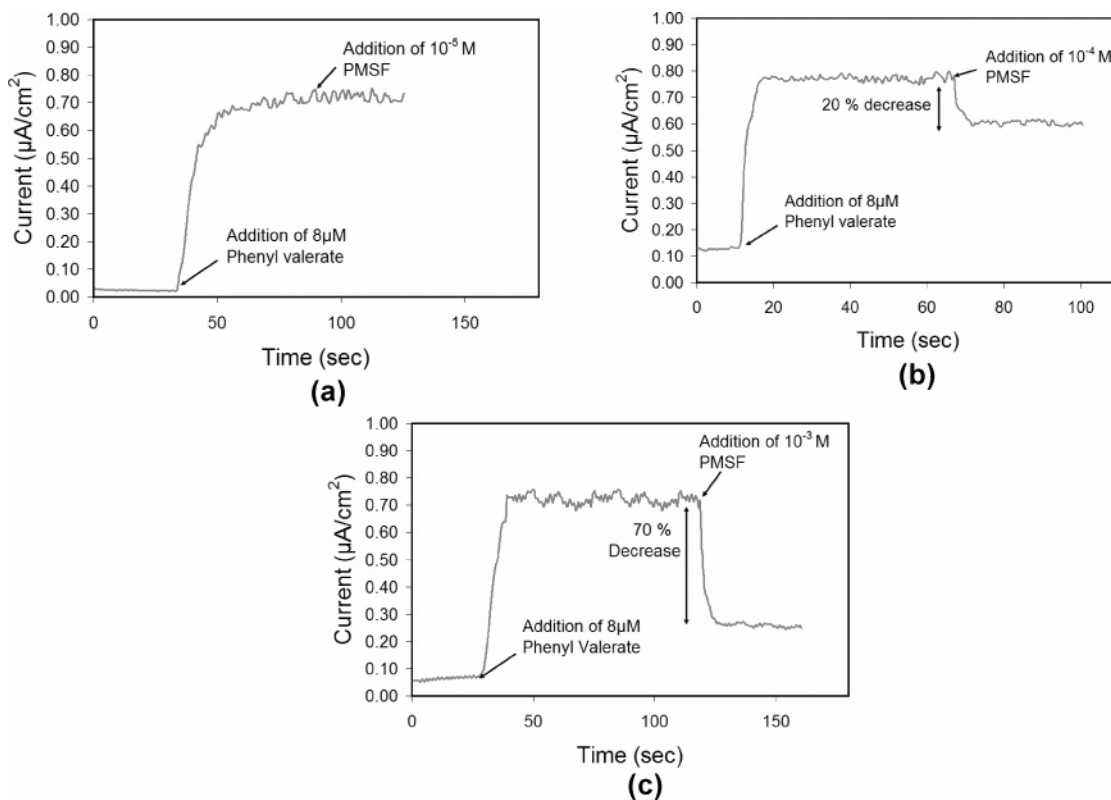


Figure 9. Current vs time response of the NEST biosensor to the addition of phenyl valerate to obtain a final phenyl valerate concentration of $8 \mu\text{M}$ followed by the addition of NEST inhibitor PMSF to obtain a final PMSF concentration of (a) 10^{-3} , (b) 10^{-4} , and (c) $10^{-3} \mu\text{M}$, in 0.1 M phosphate buffer, pH 7.0.

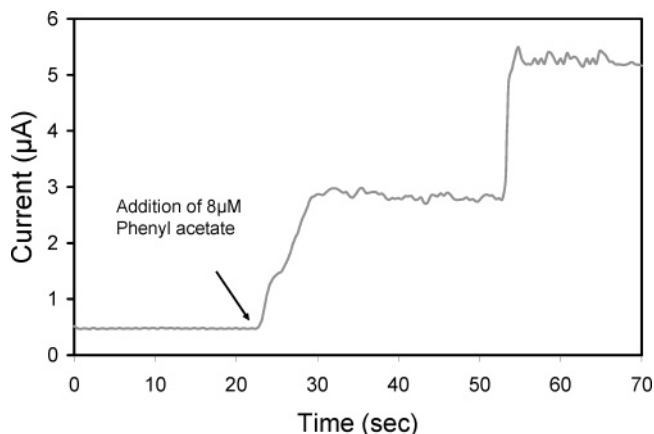


Figure 10. Current vs time response of a bienzyme electrode consisting of Tyr and AChE to the addition of aliquots of phenyl acetate to obtain final phenyl acetate concentrations as increments of $8 \mu\text{M}$ in the phosphate buffer, pH 7.0, at an applied potential of -0.1 V (vs Ag/AgCl).

CONCLUSIONS

A novel biosensor has been developed that allows the esterase activity of NEST to be measured continuously. The biosensor was fabricated using a layer-by-layer self-assembly approach to coimmobilize NEST and Tyr on a gold electrode. Ellipsometry and EIS provided evidence for the sequential assembly of the multiple layers that make up the interface. Constant potential amperometry allowed NEST's esterase activity to be measured with a rapid response time ($<10 \text{ s}$). The biosensor's response increased

Table 2. Performance of Bienzyme Electrodes Containing Tyrosinase and Different Esterases ($n = 10$ Electrodes)^a

enzyme	substrate used	average sensitivity ($\text{nA } \mu\text{M}^{-1} \text{ cm}^{-2}$)
NEST	phenyl valerate	87 ± 8
acetylcholinesterase	phenyl acetate	180 ± 25
butyrylcholinesterase	phenyl valerate	25 ± 10

^a Phenyl valerate gave the highest current sensitivity for bienzyme electrodes containing Tyr and NEST and also for bienzyme electrodes containing Tyr and BChE. Phenyl acetate gave the highest sensitivity for bienzyme electrodes containing Tyr and AChE.

linearly with the concentration of NEST's substrate (phenyl valerate) and was inhibited in a concentration-dependent manner by a known NEST inhibitor (PMSF). The versatile approach was shown to be applicable to other medically relevant esterases, including AChE and BChE.

ACKNOWLEDGMENT

The first two authors contributed equally to this work. This work was funded in part by the National Science Foundation (CTS-0609164), the U.S. Army (DAAD19-02-1-0388), the MSU Foundation, and the State of Michigan Technology Tri-Corridor program.

Received for review January 28, 2007. Accepted April 28, 2007.

AC0701684